TABLE I. Experimental and calculated relaxation times for P^{31} in Si : P. T_2^* is the free-induction decay time, T_2 the spin-echo decay time, and T_1 the spin-lattice relaxation time.

Sample	N_D (cm^{-3})	T_2^* (μsec)	T_2(expt) (msec)	T_2(calc) (msec)	T_1(msec) 1.3 °K	T_1(msec) 2.0 °K	T_1T Expt	T_1T Korringa[a]
P-1	1.4×10^{20}	20±4	7.0±0.7	3.8	130±15		0.17±0.02[b]	0.22±0.04
P-2	0.9×10^{20}	20±4	5.0±0.6	4.1	140±12	76±10	0.18±0.02	0.26±0.05
P-3	0.45×10^{20}	Signal unobservable						
P-4	0.18×10^{20}							

[a]From the Korringa relation (Ref. 4) and Knight-shift data of Ref. 1.
[b]On basis of 1.3 °K point only.

neighboring P^{31} spins.)

The values of T_1 for P^{31} represent more accurate values than the rough numbers reported in Sec. III A of Ref. 1. They are consistent with the Korringa relation, and show that Knight shift and relaxation are both determined by the hyperfine interaction of the P^{31} nuclei with the mobile conduction electrons.

*Work supported in part by Army Research Office (Durham) through Contract No. DA-ARO-D-31-124-G-1071. Early work by one of us (J. A. K.) was also supported by a grant from the Air Force Office of Scientific Research to Ohio State University under Grant No. AFOSR 1273-67.

†Present address: Naval Ordnance Laboratory, White Oak, Silver Spring, Maryland.

[1]R. K. Sundfors and D. F. Holcomb, Phys. Rev. 136, A810 (1964).
[2]W. G. Clark, Rev. Sci. Instr. 35, 316 (1964).
[3]R. K. Sundfors, Ph. D. thesis (Cornell University, 1963) (unpublished).
[4]J. Korringa, Physica 16, 601 (1950).

[5]This equation, appropriate to the case of broadening by interactions among a dilute system of randomly located spins, was derived by P. W. Anderson. See A. Abraham, *The Principles of Nuclear Magnetism* (Oxford U. P., London, 1961), pp. 125–128.

[6]This equation is derived by C. P. Slichter [*Principles of Magnetic Resonance* (Harper and Row, New York, 1963), p. 154, Eq. (31)]. We have replaced H_z of that equation by the expression $2.5\gamma_{Si}\hbar N_{Si}$. This local-field expression is derived from Eq. (1), reduced by a factor of $\frac{2}{3}$ because the mutual spin-flip contribution to the linewidth is missing for the case of unlike moments.

PHYSICAL REVIEW B VOLUME 3, NUMBER 12 15 JUNE 1971

Infrared and Raman Studies of Long-Wavelength Optical Phonons in Hexagonal MoS_2

T. J. Wieting* and J. L. Verble
Naval Research Laboratory, Washington, D. C. 20390
(Received 22 December 1970)

Infrared and Raman measurements of lattice vibrations in hexagonal MoS_2 have been made over the combined range 20–4000 cm^{-1}. Two infrared-active modes at 384 and 470 cm^{-1} and three Raman-active modes at 287, 383, and 409 cm^{-1} have been observed. Classical dielectric oscillators are fitted to the reflectivity data, which are also analyzed by means of the Kramers-Kronig relations. The degeneracy of the E_{1u} and E_{2g}^1 modes is interpreted as indicating that the layer-layer interaction is weak. All 15 optical modes are assigned to irreducible representations and their frequencies tabulated or predicted.

I. INTRODUCTION

Lattice vibrations in MoS_2 (molybdenite) have been studied by measuring the infrared reflectivity and Raman scattering from natural crystals. The semiconductor MoS_2 occupies a central position in the large class of layered compounds formed by transition metals and sulfur, selenium, or tellurium.[1] These compounds show a broad variation of properties, ranging from electrical insulators such as HfS_2 to metals such as $NbSe_2$, which is a superconductor below 7 °K. Moreover, the compounds are highly anisotropic, cleave easily along a preferred plane, and appear in a number of stacking polytypes. These properties provide an interesting basis for studies of lattice dynamics. The present paper is the second in a projected series on this class of compounds.

In Sec. II the crystal structure is presented, and the normal-mode displacements are assigned to the irreducible representations given by the authors in an earlier paper.[2] Natural MoS_2 has six

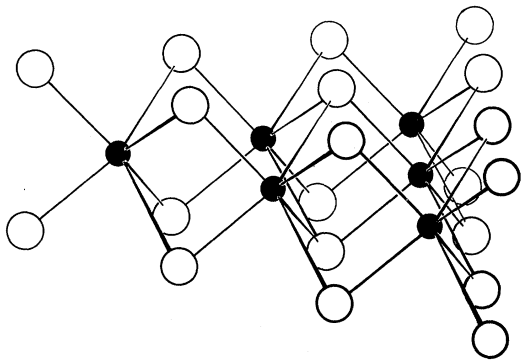

FIG. 1. Coordination of the molybdenum and sulfur atoms in a single layer of MoS_2. The molybdenum atoms are the black circles.

atoms in the primitive unit cell, and therefore 15 optical modes are allowed.

Section III gives the results of the infrared and Raman measurements. The infrared data are analyzed in two ways: First, dielectric oscillators which include a damping term proportional to the displacement velocity are fitted to the resonances in the reflectivity. Second, the Kramers-Kronig (K-K) relations are used to determine the real and imaginary parts of the dielectric function, as well as the transverse-optical (TO) and longitudinal-optical (LO) phonon frequencies. The results of these two methods are compared.

In Sec. IV the data are discussed in terms of the weak layer-layer interaction, which is an important lattice-dynamical feature of layered compounds. The frequencies of the various modes are identified or predicted, including those that are optically inactive. Finally, the approach to be taken in constructing an interatomic-force model for MoS_2 is indicated.

II. CRYSTAL STRUCTURE AND VIBRATIONAL MODES

The basic coordination unit for MoS_2 is the trigonal prism: The molybdenum atom at the center of the prism is coordinated with six sulfur atoms at the corners. A layer is composed of alternately occupied prisms placed side by side, as shown in Fig. 1. Thus each sulfur atom shares itself with three molybdenum atoms in the same layer, and no strong bonds extend across the gap between the layers.[3] This accounts for the easy mechanical cleavage along the basal plane. Although the layers are structurally identical, variation in the stacking sequence leads to the formation of polytypes.[4] In the case of hexagonal molybdenite, which is a uniaxial crystal belonging to the space group D_{6h}^4 ($P6_3/mmc$), the repeat unit in the c direction contains two layers, and the sulfur atoms in one layer are directly above the molybdenum atoms in the next. We refer to this polytype as $MoS_2(2H)$ (two layers, hexagonal). Two molecular units lie within the primitive unit cell (Fig. 2), for which the magnitudes of the translation vectors[1] are $a_1 = a_2 = a_3 = 3.160$ Å and $c = 12.29$ Å. Other useful dimensions are the interlayer gap (2.96 Å), the Mo-S bond length (2.41 Å), and the S-S distance across the gap (3.47 Å).

A group-theoretical analysis of Γ-point lattice vibrations in $MoS_2(2H)$ has already been given by the authors.[2] From these results, namely, the odd or even symmetry of the vibrations, and the type of atoms that are involved, the 18 allowed normal modes can be uniquely determined. Figure 3 shows the six modes which have atomic displacements parallel to the c axis; the degenerate basal-plane modes have analogous displacements. Also shown in Fig. 3 are the irreducible representations that belong to the normal modes.

III. EXPERIMENTAL RESULTS

A. Infrared Reflectivity

The infrared reflectivity of natural[5] MoS_2 at room temperature was obtained over the range 80–4000 cm^{-1} for $\vec{E} \perp c$, and over 200–1000 cm^{-1} for $\vec{E} \parallel c$. A modified Perkin-Elmer model 301 spectrometer was used for measurements above 100 cm^{-1}, and an interferometer was used below 100 cm^{-1}. With the former instrument a point-by-point sample-in-mirror-in procedure was followed, and the data were corrected for the reflectivity of the aluminum mirror.[6]

Samples were prepared with reflecting surfaces parallel either to the basal plane or to the c axis.

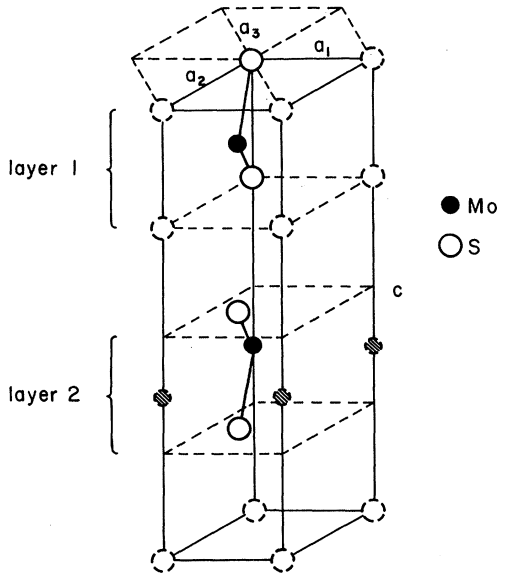

FIG. 2. Primitive unit cell of $MoS_2(2H)$.

The highest value of the basal-plane reflectivity ($\vec{E} \perp c$) was obtained using natural or cleaved surfaces. Polishing the basal-plane surface tended to lower the reflectivity in the near infrared. A diamond saw was used to cut the crystals parallel to the c axis. After polishing, the near-infrared reflectivity of the c-axis samples was 0.183 ± 0.004 for $\vec{E} \parallel c$. The value for $\vec{E} \perp c$ agreed with that obtained from the basal-plane samples. The effective size of the samples varied between 2 and 6 mm in diam.

Two infrared-active modes were observed at 384 cm^{-1} ($\vec{E} \perp c$) and 470 cm^{-1} ($\vec{E} \parallel c$).[7] The data points for these bands are plotted in Fig. 4. The solid curves in the figure represent damped classical oscillators, each of which has a complex dielectric function of the form

$$\epsilon_1 = \epsilon_\infty + \frac{4\pi\rho\omega_0^2(\omega_0^2 - \omega^2)}{(\omega_0^2 - \omega^2)^2 + (\gamma\omega_0\omega)^2} , \quad (1)$$

$$\epsilon_2 = 4\pi\rho\omega_0^2 \frac{\gamma\omega_0\omega}{(\omega_0^2 - \omega^2)^2 + (\gamma\omega_0\omega)^2} , \quad (2)$$

where ϵ_1 and ϵ_2 are the real and imaginary parts, ϵ_∞ is the high-frequency dielectric constant, ρ is the oscillator strength, γ is the damping constant, ω_0 is the resonance frequency, and ω is the frequency of the radiation. Although Eqs. (1) and (2) are given by Born and Huang[8] for an isotropic medium, they also apply to uniaxial crystals[9] that have a pair of infrared-active modes, one parallel and the other perpendicular to the axis of symmetry. The reflectivity is related to the dielectric function through the usual equations:

$$R = \frac{(n-1)^2 + k^2}{(n+1)^2 + k^2} , \quad (3)$$

$$\epsilon_1 = n^2 - k^2 , \quad (4)$$

$$\epsilon_2 = 2nk , \quad (5)$$

where n is the index of refraction and k is the extinction coefficient.

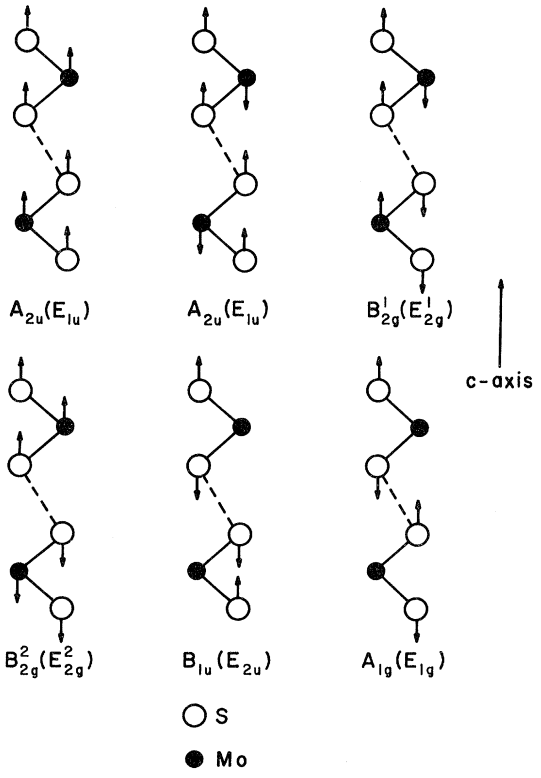

FIG. 3. Displacement vectors for the six c-axis normal modes of $MoS_2(2H)$, as viewed along the [1000] direction. Irreducible representations are assigned; those in parentheses are for the analogous basal-plane modes.

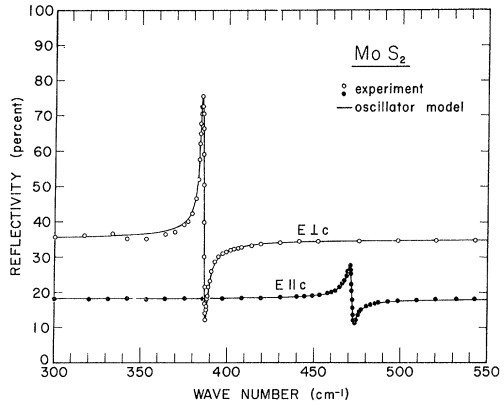

FIG. 4. Reflectivity of $MoS_2(2H)$ at room temperature for $\vec{E} \perp c$ and $\vec{E} \parallel c$. The solid curves are generated by means of the parameters of Table I and represent best fits to the reflectivity data.

Table I shows the values of the oscillator parameters for each of the polarization directions. Away from the resonance bands, the reflectivity was constant out to the limits in energy noted above. Most of the samples were optically opaque for thicknesses > 0.4 mm, except at wave numbers greater than 1000 cm^{-1}. However, even in this region the reflectivity was found to be constant, after corrections were made for multiple reflections and attenuation.

From the maximum and minimum of the modulus of the dielectric function, the TO- and LO-phonon frequencies can be obtained.[10] These are given in Table I. The longitudinal frequencies are compared with those calculated from the well-known Lyddane-Sachs-Teller relationship.[11]

A Kramers-Kronig analysis of the reflectivity data was also carried out in order to determine the real and imaginary parts of the dielectric function. Figures 5 and 6 compare the results of this analysis with the dielectric functions generated by means of

the parameters of Table I. The agreement is seen to be excellent.

From the high-frequency dielectric constants of Table I, the indices of refraction for the ordinary and extraordinary ray can be calculated: $n_o = 3.90 \pm 0.05$ and $n_e = 2.50 \pm 0.04$. Thus the birefringence is $n_e - n_o = -1.40$. Both of the indices are considerably larger than those previously reported[12, 13] and are in better agreement with the earlier work of Bailly.[14]

The index for the ordinary ray was checked using the interference-fringe method, and the value obtained for a sample 25 μ thick was $n_o = 3.9 \pm 0.2$ ($500 \leq \bar{\nu} \leq 4000$ cm^{-1}). In the fringe method the principal source of error is the measuring of the thickness of the sample. Two independent measurements were made: one with a 0.0001-in. micrometer screw, and the other indirectly by means of the density, surface area, and weight of the sample. Both gave approximately the same results (25 ± 1 μ).

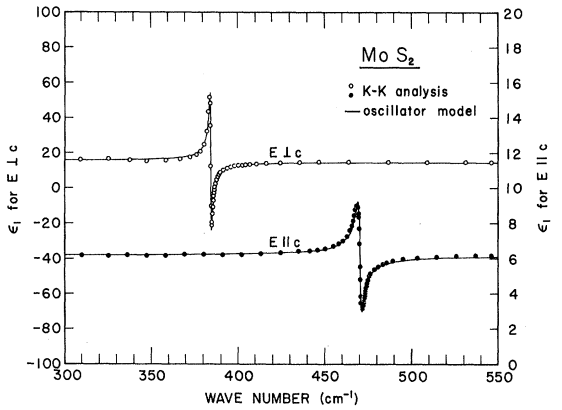

FIG. 5. Real part of the dielectric function for $MoS_2(2H)$. The data points come from a Kramers-Kronig analysis of the reflectivity, and the solid curve is a damped classical oscillator generated by means of the parameters of Table I.

B. Raman Scattering

Raman spectra were obtained using an argon-ion laser, back scatter geometry, a double monochromator, and photon-counting electronics. Three Raman lines were observed with 5145-Å laser light of about 500-mW intensity. The spectral range covered was 20–1000 cm^{-1}, and the resolution was 3 cm^{-1}. For the basal-plane crystals the angle of incidence of the focused laser beam was equal to the Brewster angle. The scattered light was collected normal to the incident beam. Normal incidence and reflection were used to obtain the Raman spectrum of the c-axis crystals.

Table II in Sec. IV shows the polarizations required for distinguishing the modes of a specific representation. However, since two of the modes have the same irreducible representation, they cannot be distinguished by the polarizations of the incident and scattered rays. Raman lines having the transformation properties of all three of the representations appeared in the recorded spectra; consequently, one of the E_{2g} modes was not observed. The frequencies[15] of the Raman lines at room temperature are 287, 383, and 409 cm^{-1}. The spectra are shown in Fig. 7. All three lines are shifted by +2 cm^{-1} at liquid-nitrogen temperature.

It is important to note how the spectra of Fig. 7 were recorded, as they preserve the relative intensities of the lines. In order to eliminate the polarization effects of the grating and optics on the recorded spectra, a polarization scrambler was inserted between the analyzer and the entrance slit of the monochromator. Basal-plane crystals were used to obtain the (xx) and (xy) spectra, and c-axis crystals were used to obtain the (zz) and (zx) spectra. For (xx) polarization a fine adjustment in the orientation of the analyzer was made by maximizing the intensity of the A_{1g} line. The spectrum was then recorded. The (xy) spectrum was obtained simply by rotating the analyzer by 90° and minimizing the intensity of the A_{1g} line. An identical procedure was followed for the (zz) and (zx) spectra. The intensity of the A_{1g} line was 440 counts/sec in the (zz) spectrum and 110 counts/sec in the (xx) spectrum. These counting rates, however, should not be compared directly, since the conditions of measurement varied somewhat in the two spectra.

TABLE I. Classical-oscillator parameters and optical-phonon frequencies ($\bar{\nu}$) for the infrared-active modes in $MoS_2(2H)$.

Polarization direction	ρ	γ	ϵ_∞	$\bar{\nu}_{TO}$(cm^{-1}) Maximum of modulus	$\bar{\nu}_{LO}$(cm^{-1}) Minimum of modulus	$\bar{\nu}_{LO}$(cm^{-1}) Lyddane-Sachs-Teller
$\vec{E} \perp c$	0.016 (±0.001)	0.0025 (±0.0002)	15.2 (±0.2)	384 (±1)	387 (±1)	386 (±1)
$\vec{E} \parallel c$	0.0024 (±0.0002)	0.005 (±0.0005)	6.2 (±0.1)	470 (±1)	472 (±1)	472 (±1)

IV. DISCUSSION

Group theory predicts two infrared- and four Raman-active modes for $MoS_2(2H)$. The group-theoretical transformation properties given in Table II agree with the polarization properties of the five experimentally observed modes. Moreover, except for the 383-cm^{-1} Raman line, the frequencies given in Table II are readily assigned to the vibrational modes of Fig. 3. The 383-cm^{-1} Raman line, however, can be assigned to either of the two E_{2g} modes, since their transformation properties are the same.

There are two basic facts that bear upon the assignment of the 383-cm^{-1} Raman line. First, the E_{1u} infrared-active mode, and one of the E_{2g} Raman-active modes, are nearly degenerate in energy. Since $MoS_2(2H)$ possesses a center of inversion, the infrared- and Raman-active modes are mutually exclusive. Thus the degeneracy either is accidental or indicates a more fundamental physical effect. The second fact is that the E_{1u} and E^1_{2g} modes in Fig. 3 differ only by an interlayer phase shift of 180°. The authors have pointed out in their previous paper[2] that if the interlayer interaction is assumed to be weak by comparison with the forces within a layer, the E_{1u} and E^1_{2g} modes will be degenerate. Indirect evidences for this assumption are the easy mechanical cleavage of MoS_2 along the basal plane, the layered crystal structure, and the nature of the interlayer bonding, which is thought to be of the van der Waals type. We therefore assume that the forces between the layers are relatively weak and assign the 383-cm^{-1} Raman line to the E^1_{2g} normal mode.

Several other consequences follow from the assumption of relatively weak interlayer forces. The frequency of the E^2_{2g} Raman-active mode, which is similar to an acoustical mode in which the restoring force is the layer-layer interaction, should be very low. The spectral limit of the Raman measurements was 20 cm^{-1}, so that the frequency of the E^2_{2g} mode is probably smaller than this. Another consequence is that the frequencies of the four inactive modes can be predicted, as they are related to active modes through an interlayer phase shift of 180° (see Fig. 3). Because of the weak layer-layer interaction, the inactive modes should have approximately the same frequencies as their conjugate active modes. The predicted frequencies are given in parentheses in Table II. A further consequence is that the normal vibrations of MoS_2 are substantially those of a single layer. Therefore the four principal frequencies of MoS_2 are 287, 384, 409, and 470 cm^{-1}. One should expect that lattice-mode degeneracy will also be present in other layer compounds.

The small values of the oscillator strengths for the infrared-active modes in MoS_2 suggest that the bonding between the molybdenum and sulfur atoms is largely covalent. This conclusion is supported by the degeneracy of the E_{1u} and E^1_{2g} modes: Weak layer-layer interactions imply that the long-range Coulomb forces, associated with charge on the atomic sites, are also weak. An interatomic-force model that incorporates only interactions within a single layer should therefore be sufficient to de-

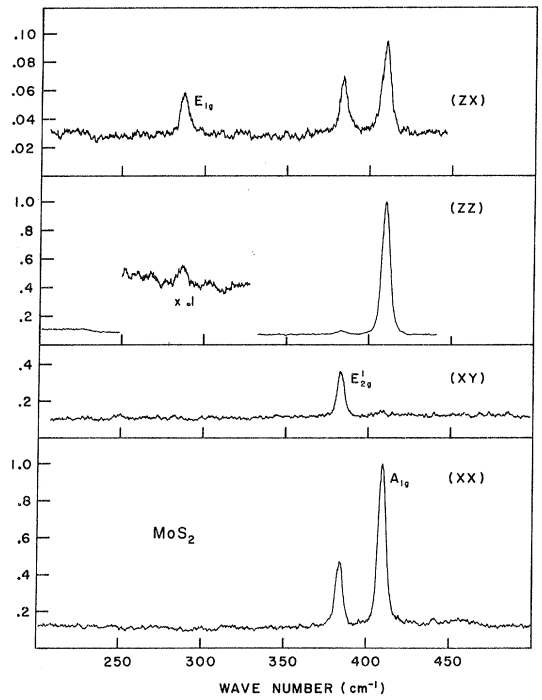

FIG. 7. Raman spectrum of $MoS_2(2H)$ at room temperature. The (zx) and (xy) spectra are normalized to the (zz) and (xx) spectra, respectively.

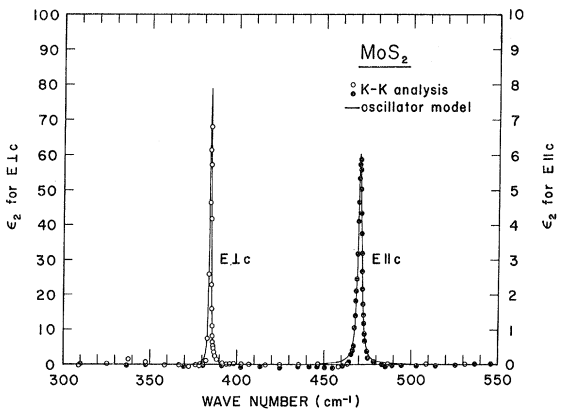

FIG. 6. Imaginary part of the dielectric function for $MoS_2(2H)$. The data points come from a Kramers-Kronig analysis of the reflectivity, and the solid curve is a damped classical oscillator generated by means of the parameters of Table I.

TABLE II. Long-wavelength lattice vibrations of $MoS_2(2H)$. The frequencies in parentheses are predicted from arguments presented in the text.

Irreducible representation	Transformation properties	Activity	Direction of vibration	Atoms involved	$\bar{\nu}$ (cm^{-1})
A_{2u}	T_z	acoustical	c axis	Mo+S	• • •
B_{2g}^2		inactive	c axis	Mo+S	(low frequency)
A_{2u}	T_z	infrared ($\vec{E} \parallel c$)	c axis	Mo+S	470
B_{2g}^1		inactive	c axis	Mo+S	(470)
A_{1g}	$\alpha_{xx}+\alpha_{yy}$, α_{zz}	Raman	c axis	S	409
B_{1u}		inactive	c axis	S	(409)
E_{1u}	T_x, T_y	acoustical	basal plane	Mo+S	• • •
E_{2g}^2	$\alpha_{xx}-\alpha_{yy}$, α_{xy}	Raman	basal plane	Mo+S	(low frequency)
E_{1u}	T_x, T_y	infrared ($\vec{E} \perp c$)	basal plane	Mo+S	384
E_{2g}^1	$\alpha_{xx}-\alpha_{yy}$, α_{xy}	Raman	basal plane	Mo+S	383
E_{1g}	α_{yz}, α_{zx}	Raman	basal plane	S	287
E_{2u}		inactive	basal plane	S	(287)

scribe the lattice dynamics of MoS_2.

The infrared and Raman data will now be compared with different types of measurements carried out by other authors. Wilson and Yoffe[1] have reported a transmission spectrum for natural MoS_2 between 300 and 5000 cm^{-1}, and interpreted the strong absorption band at 374 cm^{-1} as the TO phonon. This agrees approximately with the frequency (384 cm^{-1}) of the E_{1u} infrared-active mode in Table II. However, the indirect absorption edge,[16] which they reported to be at $\approx$ 2000 cm^{-1}, has not appeared in any of the transmission spectra which we have obtained. These measurements were undertaken in order to determine whether the reflectivity of MoS_2, which is transparent above 1000 cm^{-1}, was in fact constant (see Sec. III A). The transmission spectrum in the region 1000–4000 cm^{-1} indicated that the absorption coefficient varied as the square of the wavelength, and hence the variation was probably due to free-carrier absorption. Detailed measurements of this kind were made on a crystal 0.4 mm thick.[17]

Hall-effect and conductivity measurements by Fivaz and Mooser[18] on n-type MoS_2 have shown that the free carriers are largely confined to individual layers, and that for $T > 250$ °K they are scattered by homopolar optical phonons that modulate the thickness of the layers. From the dependence of the mobility on temperature, they predicted a phonon energy of $\approx$ 0.06 eV. This agrees moderately well with the energy of the c-axis A_{1g} phonon, which is 0.051 eV.

In a paper by Wieting and Yoffe[19] the spectral shift of the photoconductivity peak away from the exciton resonance in MoS_2 was interpreted by means of an exciton-phonon ionization model. A phonon of energy $\approx$ 0.06 eV was required to account for a shift of 0.01 eV in the photoconductivity peak. This requirement is satisfied by the dipolar A_{2u} phonon which has an energy of 0.058 eV. Moreover, the A_{2u} phonon modulates the thickness of the layers and should therefore interact strongly with delocalized excitons.

V. CONCLUSIONS

Measurements of the infrared reflectivity and Raman scattering show that the interatomic forces within a single layer are sufficient to account for the lattice dynamics of MoS_2. The stacking sequence of the layers determines the symmetry and hence the activity of the normal modes but does not appreciably affect their frequencies. Good agreement was obtained between a dielectric-oscillator and Kramers-Kronig analysis of the reflectivity data. Both analyses show that the effective charge in MoS_2 is small and that the LO-TO splitting is less than 1%.

*National Research Council Research Associate.

[1]J. A. Wilson and A. D. Yoffe, Advan. Phys. 18, 193 (1969).

[2]J. L. Verble and T. J. Wieting, Phys. Rev. Letters 25, 362 (1970).

[3]G. A. N. Connell, J. A. Wilson, and A. D. Yoffe, J. Phys. Chem. Solids 30, 287 (1969).

[4]B. B. Zvyagin and S. V. Soboleva, Kristallografiya 12, 57 (1967) [Sov. Phys. Cryst. 12, 46 (1967)].

[5]The samples were supplied by the Museum of Natural

History, Smithsonian Institution, Washington, D. C. (Catalog Nos. R402, 91779, and C288).

[6]G. Hass, J. Opt. Soc. Am. 45, 945 (1955).

[7]The 470-cm^{-1} frequency replaces the less accurate value of 466 cm^{-1} which was given in an earlier paper (see Ref. 2).

[8]M. Born and K. Huang, *Dynamical Theory of Crystal Lattices* (Oxford U. P., London, England, 1966) Sec. 10, p. 121.

[9]R. Loudon, Advan. Phys. 13, 423 (1964).

[10]I. F. Chang, S. S. Mitra, J. N. Plendl, and L. C. Mansur, Phys. Status Solidi 28, 663 (1968).

[11]R. H. Lyddane, R. G. Sachs, and E. Teller, Phys. Rev. 59, 673 (1941).

[12]B. L. Evans and P. A. Young, Proc. Roy. Soc. (London) A284, 402 (1965).

[13]R. F. Frindt and A. D. Yoffe, Proc. Roy. Soc. (London) A273, 69 (1963).

[14]R. Bailly, Am. Mineralogist 33, 519 (1948).

[15]The authors previously reported (see Ref. 2) a Raman line at 519 cm^{-1}, which has since been shown to be spurious. However, a very weak line at 287 cm^{-1} has been discovered that has the correct polarization properties.

[16]R. A. Bromley, Phys. Letters 33A, 242 (1970).

[17]Because of the low mobility ($\approx 10^2$ cm/V sec) and high carrier concentration ($\approx 10^{17}$ cm^{-3}), free-carrier absorption in MoS_2 saturates well before free-carrier dispersion in the index of refraction becomes appreciable. Moreover, the free-carrier effective mass is thought to be large and the relaxation time short. This explains why the reflectivity of MoS_2 shows no plasma dispersion at low photon energies.

[18]R. Fivaz and E. Mooser, Phys. Rev. 163, 743 (1967).

[19]T. J. Wieting and A. D. Yoffe, Phys. Status Solidi 37, 353 (1970).

PHYSICAL REVIEW B VOLUME 3, NUMBER 12 15 JUNE 1971

Detailed Study of the Γ_{15} Conduction-Band Minimum in Germanium by Photoemission and Transverse Electroreflectance

T. M. Donovan and J. E. Fischer
Michelson Laboratory, Physics Division, China Lake, California 93555

and

J. Matsuzaki* and W. E. Spicer*
Stanford University, Palo Alto, California 94305

(Received 11 January 1971)

Direct transitions occurring at the center of the Brillouin zone can be unambiguously identified by photoemission and transverse electroreflectance methods. In a material whose valence-band maximum lies at Γ, such transitions produce structure on the leading edge of the energy distribution curve (EDC) of photoemitted electrons. In transverse electroreflectance (TER), the absence of polarization dependence associated with multivalley effects provides a signature of transitions having Γ symmetry. In this paper we report three independent studies of direct transitions near 3 eV in germanium; namely, photoemission EDC, energy-derivative EDC, and polarization-dependent TER. Both photoemission experiments yield a value 2.92 $\pm$0.05 eV for the minimum separation $\Gamma_6^- - \Gamma_8^+$ at 300 °K. The TER experiment can only be performed at 80 °K or below, and gives 3.00 $\pm$ 0.05 eV for the same gap at 80 °K. The agreement among all three is perfect, assuming a temperature coefficient of -4×10^{-4} eV/°K. The spin-orbit splitting of the conduction band is observed directly in the TER spectra; we find $\Delta(\Gamma_{15}) \equiv \Gamma_8^- - \Gamma_6^- = 0.191 + 0.005$ eV. The present results are compared with recent band calculations and previous experiments.

I. INTRODUCTION AND SUMMARY

The energy position of the Γ_{15} conduction-band minimum in germanium is a sensitive testing ground for band-structure calculations. The interband energy $\Gamma_{15} - \Gamma_{25'}$ represents the lowest critical-point transition which has not been reliably fitted to experiment in the various theoretical methods, so variations in the predicted values provide a basis for critical evaluation of the calculated band structures. Such evaluation has not been possible up to now, because of the tentative nature of prior experimental determinations of $\Gamma_{15} - \Gamma_{25'}$.

We present here the results of three completely independent spectroscopic studies of single-crystal germanium which pertain to the Γ_{15} conduction band. In two of these, the energy distribution curves (EDC) of photoemitted electrons[1] were obtained for several photon energies near 3 eV; in the more recent of the two, the energy derivative of the EDC was also recorded directly,[2] allowing more accurate location of weak structure. In the third experiment, polarization-dependent transverse electroreflectance (TER) spectra[3] were recorded from 2.8 to 3.6 eV for the three principal crystallographic orientations of the electric field. Both types of experiment provide unambiguous identification of direct transitions originating at